Journal of Applied Physics

Size dependent swift heavy ion induced Au nanoparticle elongation in SiO_2 matrix

Cite as: J. Appl. Phys. **132**, 045901 (2022); https://doi.org/10.1063/5.0099164
Submitted: 15 May 2022 • Accepted: 02 July 2022 • Published Online: 25 July 2022

Spyridon Korkos, Kenichiro Mizohata, Sami Kinnunen, et al.

Journal of Applied Physics ARTICLE scitation.org/journal/jap

Size dependent swift heavy ion induced Au nanoparticle elongation in SiO_2 matrix

Cite as: J. Appl. Phys. **132**, 045901 (2022); doi: 10.1063/5.0099164
Submitted: 15 May 2022 · Accepted: 2 July 2022 ·
Published Online: 25 July 2022

Spyridon Korkos,[1,2,a)] Kenichiro Mizohata,[3] Sami Kinnunen,[1,2] Timo Sajavaara,[1,2] and Kai Arstila[1,2]

AFFILIATIONS

[1]Accelerator Laboratory, Department of Physics, University of Jyvaskyla, P.O. Box 35, FI-40014 Jyvaskyla, Finland
[2]Nanoscience Center, Department of Physics, University of Jyvaskyla, P.O. Box 35, FI-40014 Jyvaskyla, Finland
[3]Department of Physics, University of Helsinki, P.O. Box 43, FI-00014 Helsinki, Finland

Note: This paper is part of the Special Topic on Radiation Effects in Materials.
[a)]**Author to whom correspondence should be addressed:** spyridon.s.korkos@jyu.fi

ABSTRACT

The elongation of spherical Au nanoparticles embedded in SiO_2 under swift heavy ion (SHI) irradiation is an extensively studied phenomenon. The use of a TEM grid as a substrate facilitates the identification of the same nanoparticle before and after the irradiation. Since the underdensification of SiO_2 inside the ion track plays a key role, the elongation is sensitive to the matrix material properties. Therefore, we studied the elongation process of SHI irradiated Au spherical nanoparticles of various diameters (5–80 nm) embedded either in atomic layer deposition (ALD) or plasma-enhanced chemical vapor deposition (PECVD) SiO_2. The results show that a different elongation ratio is achieved depending on the particle initial size, ion fluence, and a different SiO_2 deposition method. The embedded nanoparticles in ALD SiO_2 elongate roughly 100% more than the nanoparticles embedded in PECVD SiO_2 at the biggest applied fluence (5×10^{14} ions/cm^2). On the other hand, at fluences lower than 10^{14} ions/cm^2, nanoparticles elongate slightly more when they are embedded in PECVD SiO_2.

I. INTRODUCTION

The elongation of embedded metallic nanoparticles under swift heavy ion irradiation (SHII)[1] has attracted attention in nanoscience in the last few years. Compared to the standard nanofabrication techniques, such as electron beam lithography, ion implantation, or colloidal chemistry, with SHII, it is easy to fabricate precisely aligned nanorods.[2–10] The SHII method leads to the transformation of initially spherical nanoparticles to oriented nanorods as the ion beam shaping occurs in the form of elongation in the direction of the passing swift heavy ion.

The details of the exact mechanism behind this phenomenon as well as the different steps of the elongation process are under constant debate. A general description of the mechanism behind this phenomenon could be given in the following way. The ion forms a track in the host matrix, which leads to a decrease of density in the matrix (underdensification) above, below, and around the nanoparticle. After the passage of the ion through the nanoparticle, the nanoparticle melts and the molten metal flows to the track in the matrix, resulting in elongation after cooling and recrystallization.[11–13] Full elongation typically requires hundreds or thousands of ion hits into the nanoparticle. Depending on the irradiation conditions (ion type, energy, flux, and fluence), the degree of elongation can be controlled.

One of the most promising applications for these elongated nanoparticles is in connection to their optical response.[14–17] The metallic nanostructures exhibit localized surface plasmon modes with a resonance frequency showing up a strong extinction peak in spectroscopic measurements. Within this resonance, the electric field near the nanoparticle is greatly enhanced, which yields many phenomena, such as surface-enhanced Raman scattering,[18] fluorescence,[19,20] or emission enhancement.[21] As a result, the elongated nanoparticles can act as "nanoantennas" and be used in various photonics applications,[22] such as photocatalysis, optical waveguides, and sensors.

Even if ion beam shaping has been intensively studied, the nanoparticle modification mechanism is not fully understood yet. Thus, monitoring of every step during this sample preparation procedure is needed in order to understand better this mechanism. So far, the experiments concerning the preparation of the samples have been limited to spherical metallic nanoparticles embedded in

only a few host matrices, including amorphous SiO_2,[1,3–5,7] amorphous Si_3N_4,[23–25] and sapphire (crystalline Al_2O_3).[15,26] The fabrication of the spherical nanoparticles has followed the standard techniques, i.e., electron beam lithography, ion implantation, and colloidal chemistry. Regarding the host matrices, the main deposition techniques include plasma-enhanced chemical vapor deposition (PECVD), sputtering, and thermal growth. During the irradiation, the samples are bombarded with swift heavy ions in the range of a few MeV until hundreds of MeV aiming at the elongation of the embedded nanoparticles. After the irradiation, the irradiated samples are then prepared for transmission electron microscopy (TEM) characterization in cross-sectional geometry by the standard focused ion beam (FIB) technique (TEM-lamella technique).

The TEM-lamella technique has the disadvantage that the same nanoparticle before and after the irradiation cannot be imaged. This leads to uncertainty if, for example, an elongated nanoparticle is the result of a single irradiated particle or several particles fused together when they are close to each other. In this study, this limitation of TEM lamella technology and the possibility to use a variation of nanoparticle sizes and shapes in one irradiation lead to the use of a 20 nm thick Si_3N_4 TEM window grid as a substrate. In addition, the required sample thickness for TEM imaging is limited to around 100 nm causing restrictions on the thickness of the host matrix. In the case of more than 100 nm sample thickness, a suitable etching technique, such as HF or precise RIE (reactive ion etching), can be applied to remove part of the matrix above the nanoparticles. Consequently, the comparison of the same nanoparticle before and after the irradiation can provide accurate information, necessary to the deeper understanding of the elongation process. In our very recent letter,[27] this approach was applied to study nanorod orientation due to ion irradiation.

Due to the requirement of matrix underdensification, it can be expected that the elongation is sensitive to the matrix material properties, including the composition, the density, and the concentration of impurities and nanoparticle coverage. Since the previous studies have shown that SiO_2 (gold nanoparticles in SiO_2 is the most studied system) ensures the biggest degree of elongation,[23,25] it is worth emphasizing that many SiO_2 fabrication techniques exist. For example, an atomic layer deposition (ALD) technique, which produces high quality films (uniform and conformal) with high precision of thickness, has not been investigated in connection with SHI irradiation. Since both PECVD and ALD belong to the category of depositions based on chemical reactions, it is worth investigating their different response on the SHI irradiation. Both deposition techniques are very widely used both in research and industry and, therefore, are readily available.

In this study, spherical Au nanoparticles of several diameters were embedded in SiO_2 deposited by ALD[28,29] or alternatively in SiO_2 deposited by PECVD[30] made on Si_3N_4 TEM window grids as substrates. The samples were irradiated by energetic heavy ion beams using several fluences. The purpose of this work was to study in detail the elongation of spherical nanoparticles under heavy ion irradiation in connection to their initial size and ion fluence. The effect of ALD deposited SiO_2 was compared to SiO_2 deposited by PECVD.

II. EXPERIMENTAL METHODS

A. Sample preparation

Two types of samples with SiO_2 films were fabricated using different deposition techniques. In the first type, the 50 nm of an SiO_2 film was first deposited using ALD at 200 °C on top of a TEM grid, with nine windows of 20 nm thick Si_3N_4. The ALD film was deposited with a Beneq TFS 200 cross-flow reactor using 150 Pa as the base pressure during the deposition. Nitrogen from an Inmatec PN 1150 nitrogen generator (99.999% purity) was used as a carrier gas as well as for purging between the precursor pulses. One ALD cycle consisted of subsequent pulses of (3-aminopropyl)-triethoxysilane (APTES) (Sigma-Aldrich, 99%), de-ionized water, and O_3, which were used as precursors for the deposition. APTES was heated to 95 °C in order to provide sufficient vapor pressure while H_2O was kept at room temperature, and O_3 was produced with a BMT 803 N ozone generator from O_2.[28] One ALD cycle consisted of 1.25, 0.75, and 0.9 s pulses of APTES, H_2O, and O_3, respectively. Exposure time after each pulse was 20, 18, and 15 s, and purging times were 20, 15, and 15 s, respectively. In order to grow 50 nm thick SiO_2 films, one deposition consisted of 1250 cycles (36 h). The dispersion of the chemically synthesized Au spherical nanoparticles (manufactured by Sigma-Aldrich) was accomplished on top of the layer by dropcasting. The nanoparticles were mixed from different solutions (containing different sizes) into one, and then, they were deposited from one single dispersion. The nanoparticle diameter varied between 5 and 80 nm, with a 5 nm step. In order to embed the nanoparticles, another 50 nm SiO_2 thin film was deposited using ALD with the same parameters.

In the second type of samples, SiO_2 films were deposited using PECVD at 200 °C. A Plasmalab80Plus system, manufactured by Oxford Instruments, was used to deposit SiO_2 with silane (SiH_4 in Ar) and nitrous oxide (N_2O) as precursors. The chamber was pre-heated and purged with N_2 for 2 min. The working pressure during the process was 133 Pa. The growth rate of the deposited film was 50 nm/min.

Summarizing the structure of the samples, the total thickness was 120 nm, which fulfilled the requirements for TEM imaging. A set of samples were fabricated with an additional step of post-deposition annealing at 900 °C for 30 min with N_2 flow at a conventional furnace since the thermal treatment (annealing) is known to improve the SiO_2 film properties.[31,32] For comparison, Fig. 1 presents a macroscopic view of a TEM grid as well as optical microscope images of this grid.

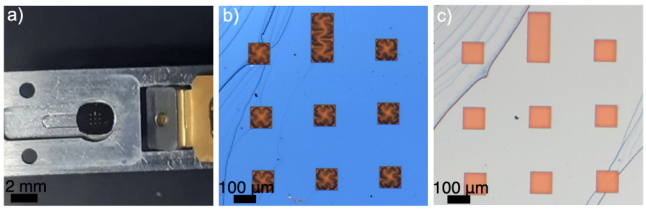

FIG. 1. (a) Photo of a TEM grid and optical microscope images of a TEM grid with SiO_2 deposited (b) by PECVD and (c) by ALD.

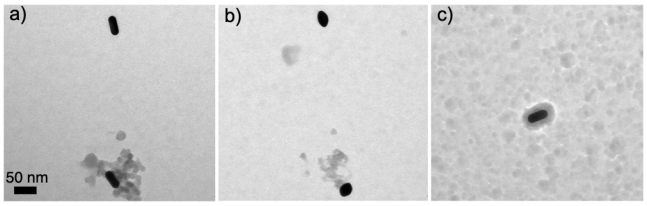

FIG. 2. TEM images of gold nanorods (a) before embedding them inside SiO_2 and (b) after embedding them inside SiO_2 deposited at 300 °C and the etching part of SiO_2. (c) TEM image of a gold nanorod after SiO_2 deposition at 200 °C.

Additional Si substrate was present in the depositions in order to investigate the properties of grown SiO_2 films. Several material characterization techniques can be applied to study these properties as discussed later.

The selection of an SiO_2 deposition temperature depends on the temperature induced shape change of not embedded gold nanoparticles. Gold nanoparticles are observed to modify at 300 °C, leading to the conclusion of choosing a lower deposition temperature than 300 °C. Figures 2(a) and 2(b) show the shape change of the nanorods after SiO_2 deposition at 300 °C. As a result, lower deposition temperatures were tested, and deposition at 200 °C showed that nanorods do not significantly change shape [Fig. 2(c)].

The effect of the post-deposition annealing on the embedded nanoparticles was investigated as well. As seen in Fig. 3, in which gold nanorods on a bulk Si substrate are imaged before and after annealing at 900 °C and etching of top SiO_2, there is no significant change even after annealing at 900 °C.

B. Sample irradiation

The heavy ion irradiation of the samples was performed with 50 MeV $^{127}I^{9+}$ ions at the TAMIA 5 MV tandem accelerator at the Helsinki Accelerator Laboratory (University of Helsinki). The angle of incidence was 45°, and several fluences from 10^{13} to 5×10^{14} ions/cm^2 were applied at room temperature. During the irradiation, the beam was raster scanned over a 2×2 cm^2 area by magnetic deflectors, and the beam current was measured by a beam profilometer placed in front of the sample. The TEM grids were mounted on silver plates using a conductive carbon paste to avoid any damage by overheating during the irradiation. All of the nine windows in a TEM grid were covered by the beam spot area of 1 cm^2. However, at high enough fluences, there is a risk for the windows to break.

Similar experiments had been performed initially where SiO_2 films were so thick that the etching part of the SiO_2 layer was essential. On top of a TEM grid with nine windows of 20 nm thick Si_3N_4, a 30 nm PECVD SiO_2 film was the first deposited at 200 °C. Then, chemically synthesized Au spherical nanoparticles with diameter varying from 5 to 80 nm were dispersed on top of the film. Finally, another SiO_2 film with 200 nm thickness was deposited in order to embed the nanoparticles. For these samples with a thicker SiO_2 film, heavy ion irradiation was performed with a 383 MeV $^{84}Kr^{16+}$ beam from the K-130 cyclotron at the Jyväskylä Accelerator Laboratory (University of Jyväskylä) in 45° incidence with several fluences at room temperature.

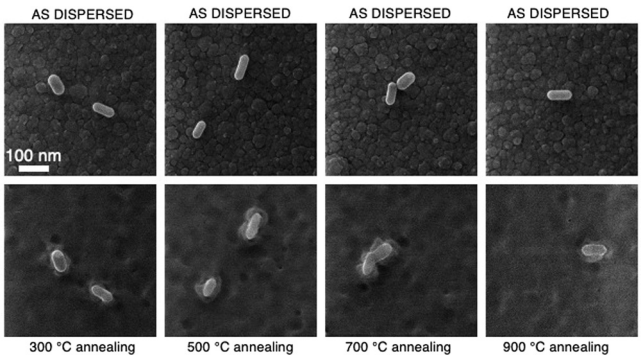

FIG. 3. Helium ion microscope (HIM) images of nanorods embedded in PECVD SiO_2 before and after annealing at various temperatures. The top images show nanorods before the deposition of the second layer on the top, and the bottom images show the same nanorods after annealing and etching of the excessive layer by RIE.

C. Sample characterization

The samples were imaged with a JEOL-JEM 1400 TEM operated at 120 kV. Before the irradiation, the samples were imaged from the top without tilting the TEM stage, but after the irradiation, the electron beam direction should be perpendicular to the ion beam direction to get the full information from an elongated nanoparticle.

Prior to irradiation of the samples with a Kr beam, the TEM imaging took place before the deposition of the second SiO_2 film. After the irradiation, around 150 nm of SiO_2 were etched by RIE to accomplish the TEM imaging. In Fig. 4, TEM images from a sample irradiated at the highest applied fluence (2×10^{14} ions/cm^2) are shown.

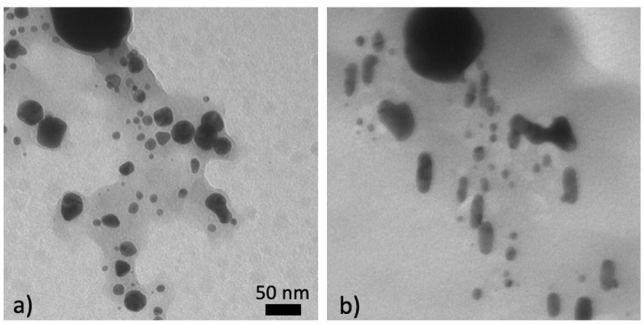

FIG. 4. TEM images of a 20 nm Si_3N_4/30 nm PECVD SiO_2/NPs/200 nm PECVD SiO_2 sample irradiated at 2×10^{14} ions/cm^2 fluence with 383 MeV ^{84}Kr ions. The images were taken (a) from the top before the irradiation and (b) perpendicular to the ion beam direction.

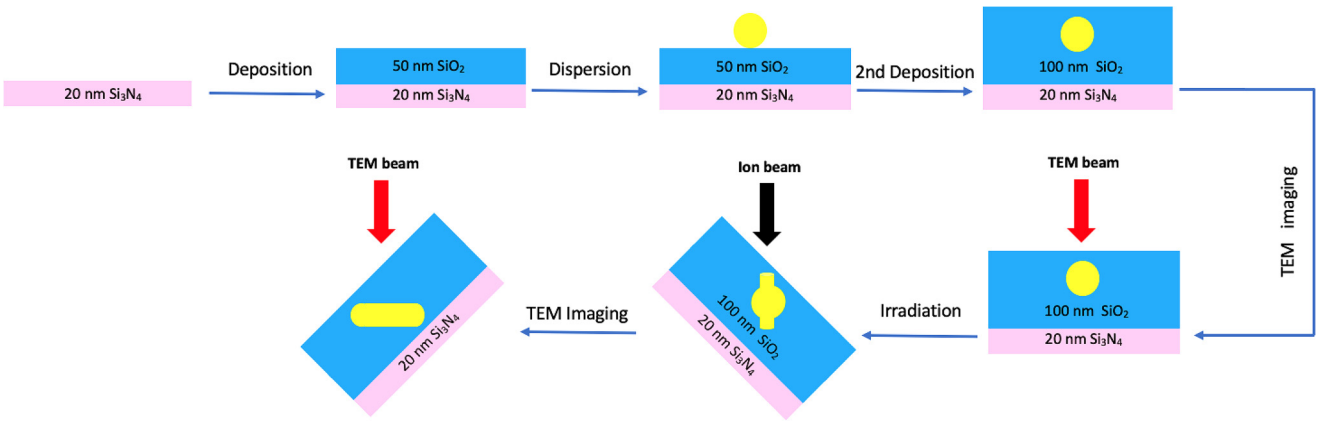

FIG. 5. Schematic representation of sample preparation, irradiation, and imaging using TEM.

It is obvious that there is information missing if this procedure is followed, such as how the nanoparticles are enclosed by the SiO_2 layer and the impact of the ion beam on the film since most of that has been removed. Consequently, these reasons and the fact that the additional film thickness does not affect significantly the elongation process led to the production of the samples with thickness thin enough to allow the TEM imaging without an etching step. All the steps of the procedure, where samples were irradiated with a ^{127}I beam, are shown in Fig. 5.

An image segmentation code was written with Python to measure the dimensions of the nanoparticles before and after the irradiation (Fig. 6).

A more detailed analysis of the film properties can be reached by means of advanced material characterization techniques,

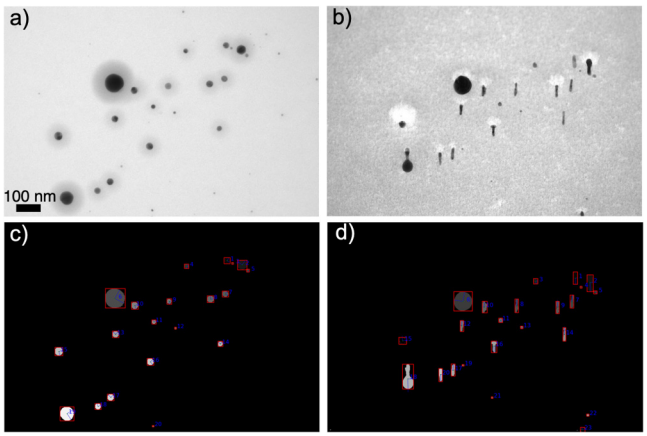

FIG. 6. TEM images of the 900 °C annealed 20 nm Si_3N_4/50 nm ALD SiO_2/NPs/50 nm ALD SiO_2 sample irradiated with a 50 MeV ^{127}I beam at 5×10^{14} ions/cm^2 fluence, which were taken (a) from the top before the irradiation and (b) perpendicular to the ion beam direction. Corresponding segmented images (c) and (d).

including time-of-flight elastic recoil detection analysis (ToF-ERDA) and x-ray reflectivity (XRR). ToF-ERDA is an ion beam analysis technique capable of determining the composition of a thin film. ToF-ERDA measurements were accomplished with the use of a 1.7 MV Pelletron accelerator.[33] In measurements, a $^{63}Cu^{6+}$ beam of 11.9 MeV energy was used. The analysis of the measurements was done using the Potku software.[34]

XRR measurements were performed in order to reveal information about the thickness, density, and roughness of the SiO_2 films. A PANalytical X'Pert Pro Alpha 1 MPD x-ray powder diffractometer setup to x-ray reflectivity was used with a Cu $K\alpha_1$ x-ray source ($\lambda = 0.154\,056$ nm, V = 45 kV, I = 40 mA). The analysis of the samples was done with GenX open software. The experimental data are reproduced by changing simulation parameters, from which the values of the thickness, density, and roughness of the SiO_2 film were extracted.

III. RESULTS

A. Properties of SiO_2 films grown using PECVD and ALD

Already, the optical microscope images in Fig. 1 show a clear difference between TEM grids with ALD and PECVD SiO_2 coatings. ALD SiO_2 has a smooth surface, but in PECVD SiO_2, surface tensions appear. Another basic difference is the way nanoparticles are enclosed by the films. In Fig. 7, two images of nanoparticles embedded either in PECVD or in ALD before irradiation are shown. We observe that around the nanoparticles, an area of darker contrast has been formed, and possible explanation could be that the nanoparticles act as nucleation sites for the growth of SiO_2. These regions are much more pronounced in PECVD SiO_2, in which grains could be observed,[35] compared to more uniform ALD SiO_2.

The elemental composition of the samples was extracted from coincidence time-of-flight and energy data (Fig. 8). ToF-ERDA depth profiles are shown for annealed and as-deposited PECVD (Fig. 9) and ALD (Fig. 10) samples. Depth profiles for the as-deposited PECVD sample [Fig. 9(a)] show that the SiO_2 is

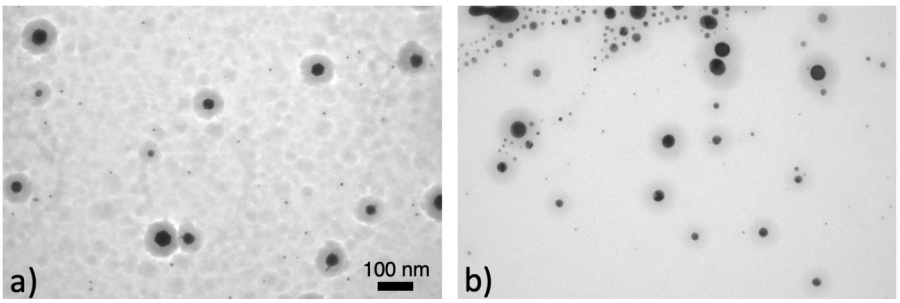

FIG. 7. TEM images of nanoparticles embedded in SiO_2 grown using (a) PECVD and (b) ALD.

stoichiometric with elemental ratio O/Si = 2.06 ± 0.02. Apart from silicon and oxygen, the film contains a significant amount of hydrogen impurity (7.6 at. %), which most probably originates from the silane precursor, and a small amount of other impurities, such as nitrogen (originated most likely from the nitrous oxide precursor), carbon, and sodium [coming from the phosphate buffer solution (PBS) of nanoparticles]. Gold can be detected as well because of the gold nanoparticles embedded inside. Depth profiles of an annealed PECVD sample [Fig. 9(b)] show that SiO_2 is oxygen poor with elemental ratio O/Si = 1.88 ± 0.02. Additionally, it contains a small amount of the same impurities as the as-deposited SiO_2, but hydrogen concentration has reduced significantly (<0.1 at. %).

The same behavior is visible in as-deposited and annealed ALD samples as well. Depth profiles for an as-deposited ALD sample [Fig. 10(a)] show that SiO_2 is nearly stoichiometric with elemental ratio O/Si = 2.07 ± 0.02. Regarding impurities, the film contains a significant amount of hydrogen (6.5 at. %) originating from APTES and water precursors and a small amount of other impurities (less than 1 at. %), including nitrogen (originating from the APTES) and carbon. Gold is again visible in the film. Depth profiles of an annealed ALD sample [Fig. 10(b)] show that SiO_2 is stoichiometric with elemental ratio O/Si = 1.97 ± 0.02. It contains a small amount of the same impurities than as-deposited SiO_2, but hydrogen concentration has again dropped (<0.2 at. %). The number of gold nanoparticles embedded in SiO_2 (1.4×10^7–1.1×10^8 nanoparticles/cm^2) was

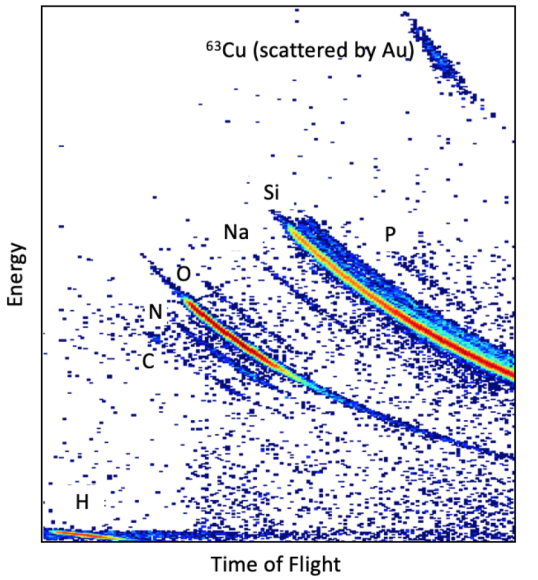

FIG. 8. Coincidence time-of-flight and an energy histogram of a ToF-ERDA measurement from an Si/50 nm PECVD SiO_2/NPs/50 nm PECVD SiO_2 as-deposited sample.

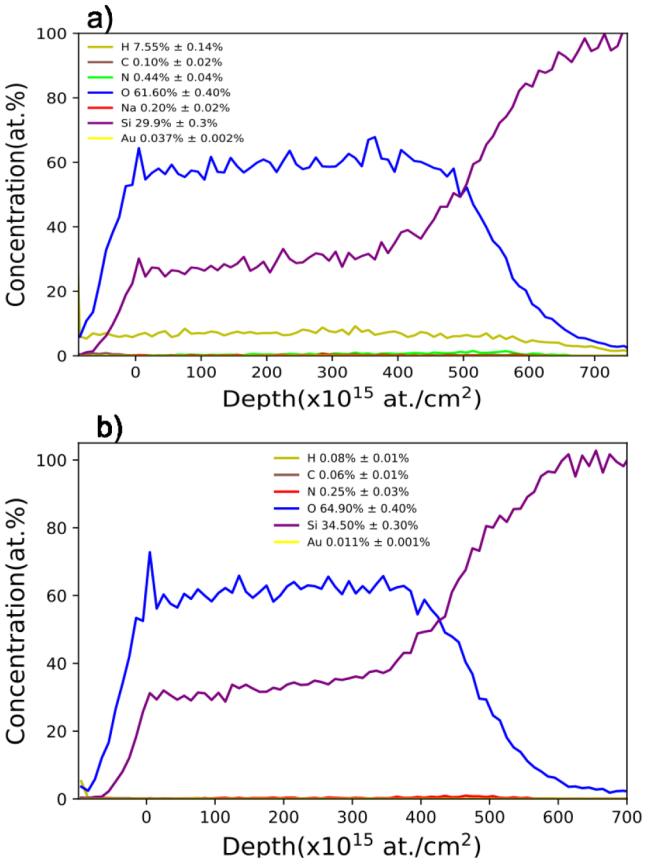

FIG. 9. ToF-ERDA depth profiles of an Si/50 nm PECVD SiO_2/NPs/50 nm PECVD SiO_2 (a) as-deposited sample and (b) annealed sample.

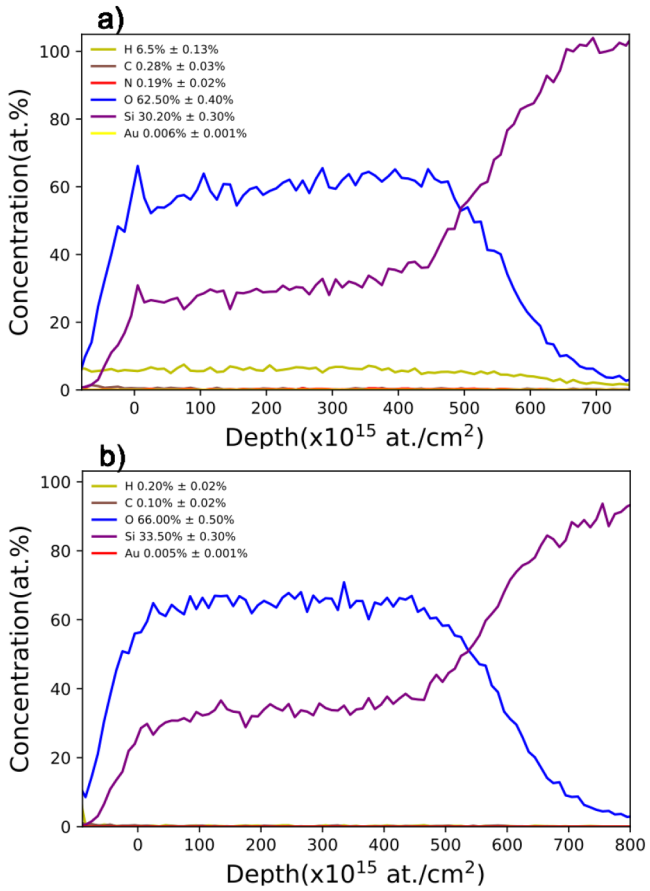

FIG. 10. ToF-ERDA depth profiles of an Si/50 nm ALD SiO_2/NPs/50 nm ALD SiO_2 (a) as-deposited sample and (b) annealed sample.

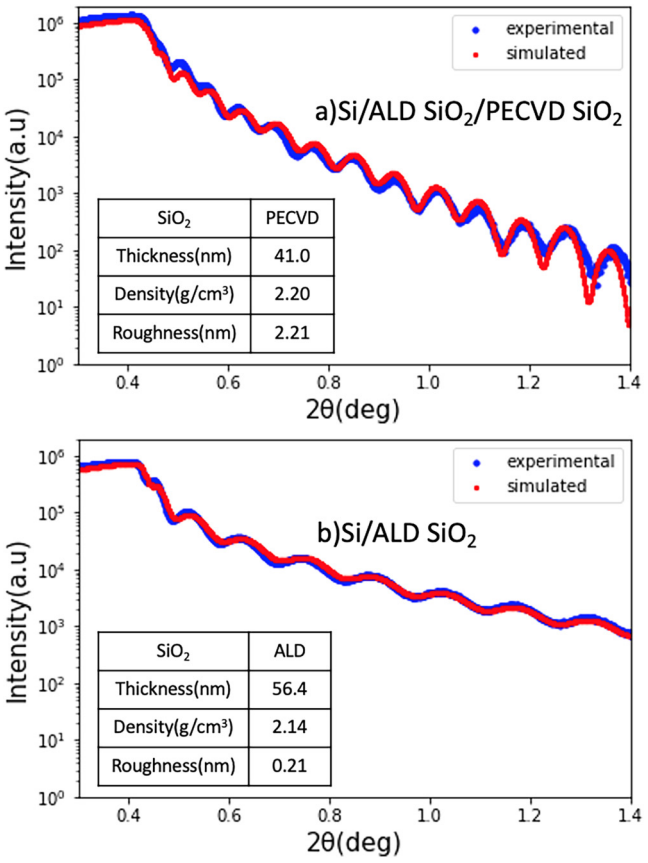

FIG. 11. Measured and simulated XRR curves of (a) an Si/50 nm ALD SiO_2/50 nm PECVD SiO_2 as-deposited sample and (b) an Si/50 nm ALD SiO_2 as-deposited sample. In each graph, there is a table with the measured quantities for each film.

calculated from atomic concentrations of gold for all the samples. This result tells that nanoparticles have a low average areal density covering less than 0.1% of the area.

In Fig. 11(a), the experimental and simulated curves from XRR data are shown for an Si/50 nm ALD SiO_2/50 nm PECVD SiO_2 sample. The density of PECVD SiO_2 was measured to be $2.20 \pm 0.06\,g/cm^3$ and the roughness 2.21 ± 0.10 nm. The measured thickness was 41.0 ± 0.9 nm. In Fig. 11(b), the experimental and simulated curves obtained by XRR are shown for an Si/50 nm ALD SiO_2 sample. The density of ALD SiO_2 was measured to be $2.14 \pm 0.05\,g/cm^3$ and the roughness 0.21 ± 0.09 nm. The measured thickness of the film was 56.4 ± 0.7 nm, which is close to the goal thickness. In order to get the information for the PECVD layer, we used the extracted parameters from the ALD-only fit and then we fit the PECVD layer.

B. Irradiation with a 50 MeV $^{127}I^{9+}$ beam

Several fluences between 10^{13} and 5×10^{14} ions/cm^2 were applied to investigate the evolution of the elongation of nanoparticles embedded in SiO_2 deposited either by ALD or PECVD. Additionally, the annealing process before the irradiation was carried out in order to see if the change in the matrix properties has any impact on the irradiation results. In Fig. 12, the average elongation ratio (length/width) vs the initial nanoparticle diameter is presented for all the samples.

Initially, spherical nanoparticle diameters varied between 5 and 80 nm. During the images analysis, they were classified in the ranges of 5 nm, i.e., 5–10, 10–15, 15–20 nm, etc. The experimental results show that there is a variation in the nanoparticle shape change for the same initial size, which is in accordance with the earlier study.[25] The elongation ratio with uncertainties is shown in Tables I (PECVD SiO_2) and II (ALD SiO_2). A standard deviation of the measured variable was used to express the variation of the ratio from its mean value. The number of particles in different size ranges varied between 10 and 100. Figures 13–19 show nanoparticles with the highest elongation ratio in each range before and after irradiation.

Single nanoparticles irradiated at lower fluences ($\leq 10^{14}$ ions/cm^2) are shown either from the as-deposited samples

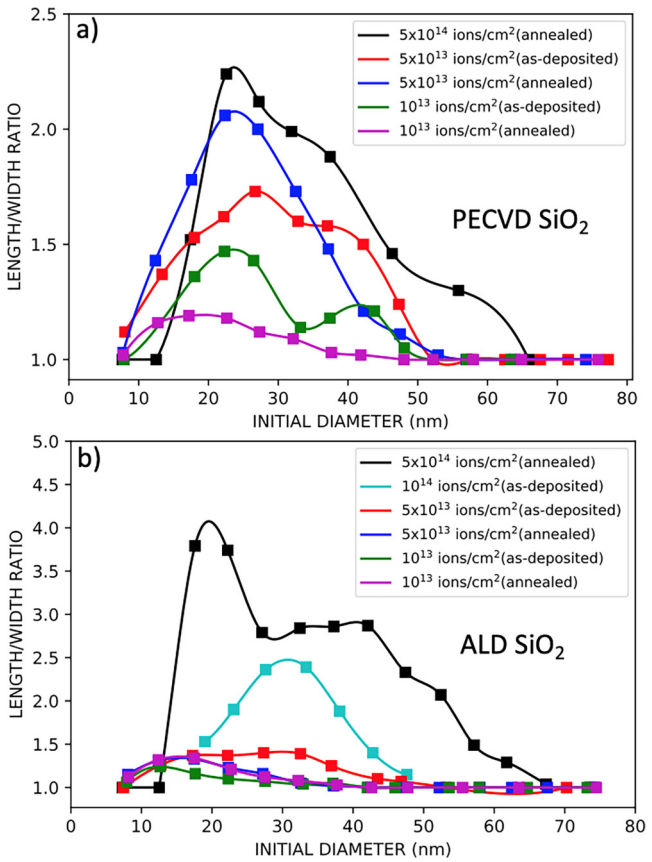

FIG. 12. Representation of the average ratio (length/width) vs the initial diameter of the elongated nanoparticles after 50 MeV ^{127}I irradiation at fluences between 10^{13} and 5×10^{14} ions/cm^2. The nanoparticles are embedded in (a) PECVD SiO_2 and (b) ALD SiO_2. The uncertainties are left out from the image for clarity.

or from the annealed samples in Figs. 13–17. Comparing the annealed and as-deposited samples at the same fluence, the elongation ratio is similar. Moreover, regarding the different deposition techniques, elongated nanoparticles in PECVD samples present a slightly higher elongation ratio for fluences $\leq 5 \times 10^{13}$ ions/cm^2.

The as-deposited PECVD and ALD samples did not withstand irradiation for the highest fluence at 5×10^{14} ions/cm^2, and most of the windows broke during the irradiation. The same problem appeared also for the annealed PECVD sample as we were able to track only a few nanoparticles after irradiation. As a result, images were collected from nanoparticles that had not been imaged before the irradiation. For the pre-imaged nanoparticles, the volume was almost the same before and after irradiation. In case the original nanoparticle was not imaged, we assumed the volume of the elongated nanoparticles as a cylinder and compared it with their spherical volume before the irradiation in order to find their initial diameter. As for the annealed ALD sample, it had intact windows with plenty of same nanoparticles imaged before and after the irradiation with TEM.

In Figs. 18 and 19, those nanoparticles with the highest elongation ratio in each range are shown. For the PECVD sample, only a few nanoparticles before the irradiation are shown. Comparing the different deposition techniques, the highest elongation ratio is achieved for ALD samples. However, the nanorods embedded in ALD SiO_2 elongate so much that some of them become unstable and tend to break up into smaller fragments, which has also been reported before[36] and is related to the inverse Ostwald ripening.[37–40]

Particularly, some of the biggest elongated nanoparticles in ALD SiO_2 (after 35 nm initial diameter) present unconventional morphologies. Between 35 and 45 nm initial diameter, the irradiated nanoparticles have obtained a shape resembling nanorod. One nanoparticle (35–40 nm) is bigger in the sides than in the middle, while the other is bigger in one side. Subsequently, for nanoparticles with diameters between 45 and 65 nm, the irradiation causes only part of them to elongate.

By increasing the fluence, the elongation ratio of the nanoparticles (Fig. 20) increases and the biggest nanoparticles also change.

TABLE I. Elongation (length/width) ratio for nanoparticles embedded in annealed (ann.) and as-deposited (as-dep.) PECVD SiO_2 samples regarding the initial diameter and fluence.

(nm)	10^{13} (ann.)	10^{13} (as-dep.)	5×10^{13} (ann.)	5×10^{13} (as-dep.)	5×10^{14} (ann.)
5–10	1.02 ± 0.02	1.00 ± 0.00	1.03 ± 0.03	1.12 ± 0.12	1.0 ± 0.0
10–15	1.16 ± 0.12	…	1.43 ± 0.22	1.37 ± 0.29	1.0 ± 0.0
15–20	1.19 ± 0.09	1.36 ± 0.32	1.78 ± 0.38	1.53 ± 0.30	1.52 ± 0.52
20–25	1.18 ± 0.10	1.47 ± 0.45	2.06 ± 0.35	1.62 ± 0.38	2.24 ± 0.70
25–30	1.12 ± 0.06	1.43 ± 0.38	2.00 ± 0.38	1.73 ± 0.32	2.12 ± 0.32
30–35	1.09 ± 0.07	1.14 ± 0.14	1.73 ± 0.34	1.60 ± 0.29	1.99 ± 0.54
35–40	1.03 ± 0.03	1.18 ± 0.18	1.48 ± 0.17	1.58 ± 0.26	1.88 ± 0.43
40–45	1.02 ± 0.02	1.21 ± 0.20	1.21 ± 0.13	1.50 ± 0.39	…
45–50	1.05 ± 0.05	1.0 ± 0.0	1.11 ± 0.11	1.24 ± 0.20	1.46 ± 0.05
50–60	1.0 ± 0.0	1.0 ± 0.0	1.0 ± 0.0	1.0 ± 0.0	1.30 ± 0.30
60–70	1.0 ± 0.0	1.0 ± 0.0	1.0 ± 0.0	1.0 ± 0.0	1.0 ± 0.0
70–80	1.0 ± 0.0	…	1.0 ± 0.0	1.0 ± 0.0	…

TABLE II. Elongation (length/width) ratio for nanoparticles embedded in annealed (ann.) and as-deposited (as-dep.) ALD SiO_2 samples regarding the initial diameter and fluence.

(nm)	10^{13} (ann.)	10^{13} (as-dep.)	5×10^{13} (ann.)	5×10^{13} (as-dep.)	10^{14} (as-dep.)	5×10^{14} (ann.)
5–10	1.12 ± 0.12	1.06 ± 0.06	1.15 ± 0.15	1.0 ± 0.0	…	1.0 ± 0.0
10–15	1.32 ± 0.14	1.24 ± 0.12	1.31 ± 0.24	1.26 ± 0.20	…	1.0 ± 0.0
15–20	1.34 ± 0.19	1.16 ± 0.09	1.33 ± 0.15	1.37 ± 0.21	1.53 ± 0.0	3.79 ± 1.82
20–25	1.21 ± 0.11	1.10 ± 0.08	1.23 ± 0.14	1.37 ± 0.23	1.90 ± 0.05	3.74 ± 1.61
25–30	1.12 ± 0.10	1.07 ± 0.07	1.16 ± 0.08	1.40 ± 0.17	2.36 ± 0.17	2.84 ± 1.03
30–35	1.08 ± 0.07	1.04 ± 0.04	1.05 ± 0.05	1.39 ± 0.12	2.39 ± 0.26	2.86 ± 1.25
35–40	1.03 ± 0.03	1.05 ± 0.05	1.03 ± 0.03	1.25 ± 0.18	1.88 ± 0.05	2.86 ± 1.25
40–45	1.0 ± 0.0	1.0 ± 0.0	1.0 ± 0.0	1.10 ± 0.05	1.40 ± 0.25	2.87 ± 0.89
45–50	1.0 ± 0.0	1.0 ± 0.0	1.0 ± 0.0	1.07 ± 0.07	1.15 ± 0.04	2.33 ± 0.53
50–55	1.0 ± 0.0	1.0 ± 0.0	1.0 ± 0.0	1.0 ± 0.0	…	2.07 ± 0.74
55–60	1.0 ± 0.0	1.0 ± 0.0	1.0 ± 0.0	1.0 ± 0.0	…	1.49 ± 0.49
60–65	1.0 ± 0.0	1.0 ± 0.0	1.0 ± 0.0	1.0 ± 0.0	…	1.29 ± 0.26
65–70	1.0 ± 0.0	1.0 ± 0.0	1.0 ± 0.0	1.0 ± 0.0	…	1.04 ± 0.04
70–80	1.0 ± 0.0	1.0 ± 0.0	1.0 ± 0.0	1.0 ± 0.0	…	1.0 ± 0.0

The threshold fluence for larger elongation is higher for ALD samples than PECVD. Additionally, smaller nanoparticles elongate slightly more in both cases.

IV. DISCUSSION

A. Dependence of elongation on fluence and nanoparticle initial size

The results show that the elongation depends strongly on the irradiation fluence and the nanoparticle initial size. The lower fluences ($\leq 5 \times 10^{13}$ ions/cm^2) favor the elongation of the smallest nanoparticles, smaller than 50 nm, because the deposited energy is not high enough to elongate the larger ones. On the other hand, for higher fluences ($\geq 10^{14}$ ions/cm^2), the deposited energy by the ion irradiation is high enough to elongate bigger nanoparticles as well. However, when the smallest nanoparticles (<15 nm), which have already started elongating, reach the higher fluences, they start to shrink and reshape back toward a spherical shape or they can disintegrate completely. This significant volume change can be explained by the fact that the irradiation fluence is too high and prevent them from elongation. According to Peña-Rodríguez *et al.*,[41] the constituent atoms of the disintegrated nanoparticles are absorbed by the larger ones (Ostwald ripening) or form new particles, but there is no experimental evidence of that in the present study. In the case of nanoparticles with a diameter smaller than 10 nm, there is basically no elongation and only a few nanoparticles show a small shape change.

The last observation can be related to the value of the ion track diameter. If the nanoparticle has a diameter less than the ion track diameter, it cannot elongate or elongate much less than the bigger ones.[42] The track diameter limits as well the minimum width that an elongated nanoparticle can reach. According to Mota-Santiago *et al.*,[25] the diameter of an ion track formed in SiO_2

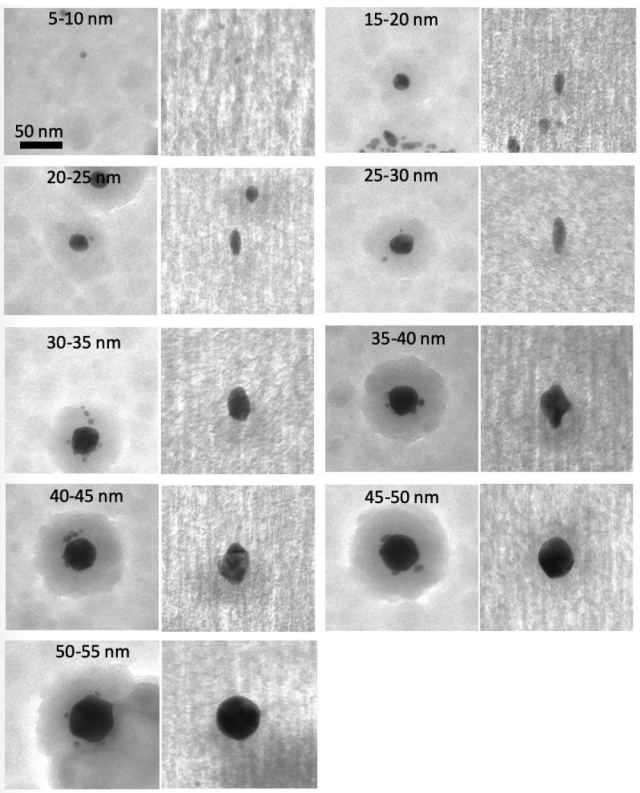

FIG. 13. TEM images of nanoparticles sandwiched between two 50 nm PECVD SiO_2 layers (as-deposited). The samples were irradiated with ^{127}I at a fluence of 10^{13} ions/cm^2 and imaged before (left) and after (right) the irradiation.

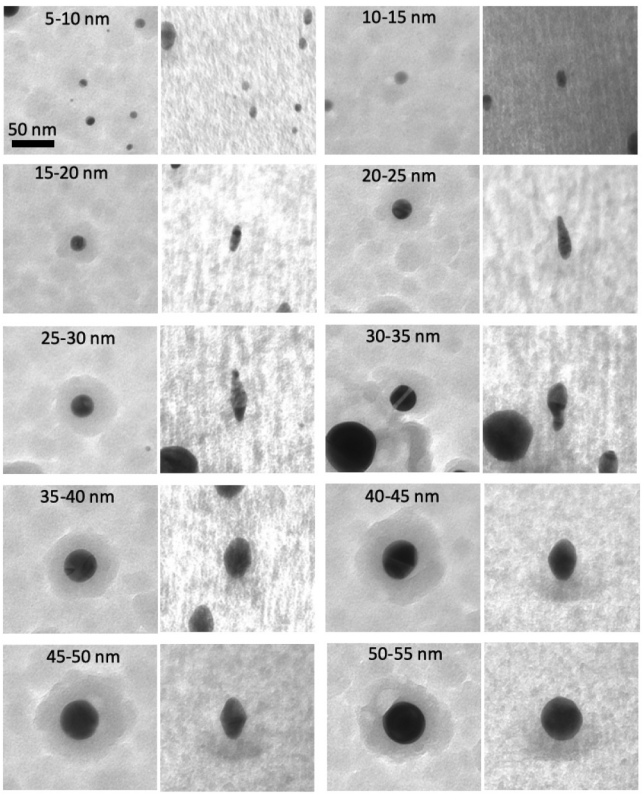

FIG. 14. TEM images of nanoparticles sandwiched between two 50 nm PECVD SiO_2 layers (annealed after the deposition). The samples were irradiated with ^{127}I at a fluence of 5×10^{13} ions/cm^2 before (left) and after (right) the irradiation.

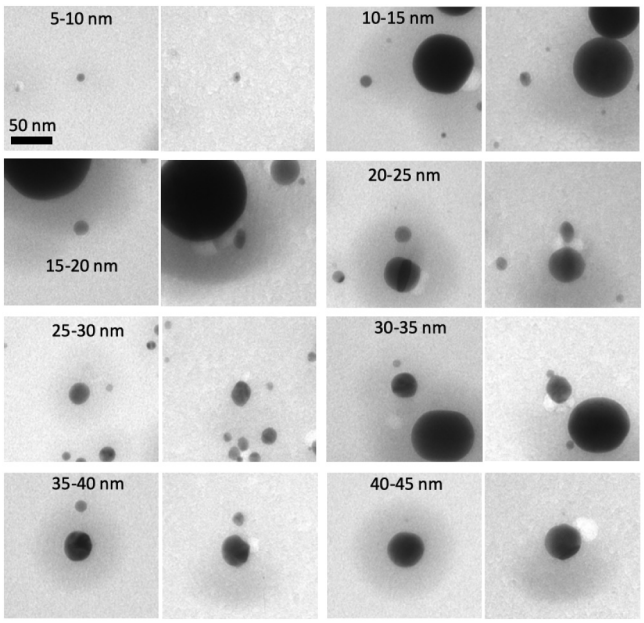

FIG. 15. TEM images of nanoparticles sandwiched between two 50 nm ALD SiO_2 layers (annealed after deposition). The samples were irradiated with ^{127}I at a fluence of 10^{13} ions/cm^2 before (left) and after (right) the irradiation.

irradiated with a 185 MeV Au beam was measured to be 10.8 nm by SAXS (small angle x-ray scattering) measurements. In this study, nanoparticles of diameter between 7 and 8 nm are the smallest that can elongate and minimum elongation width was found to have approximately the same value. This observation, in combination with the smaller deposited energy in these experiments, implies that the ion track diameter for 50 MeV ^{127}I is less than the 10.8 nm reported in the literature. Additionally, their small size and consequently a small possibility of a significant amount of ions hitting them (8–40 ion hits/10^{13}–5×10^{13} ions/cm^2) affect the elongation.

Elongation results can give additional information about the correlation between the initial particle size and the particle deformation path in the SiO_2 matrix.[7] At the highest applied fluence, nanoparticles of diameter less than 15 nm disintegrate either completely and disappear or disintegrate partially and remain spherical. At range from a 15 to 45 nm diameter, they melt completely during the ion impact and transform to nanorods along the ion beam direction after multiple impacts. At range from 45 to 65 nm, they are partially molten and the elongation occurs as an elongated part attached to a sphere. Finally, for larger nanoparticles (>65 nm), there is negligible deformation because the ion energy is not high enough to melt them. Comparing these results with Rizza's work,[7] nanoparticles of diameter up to 30 nm are completely molten, while in our case, nanoparticles of diameter up to 45 nm melt completely. This difference arises from the composition of the matrix and the irradiation conditions. In this kind of studies, SiO_2 thickness does not need to be hundreds of nanometers like in previous studies,[7,17,23,25] but 100 nm thickness is enough.

B. Effect of the SiO_2 deposition technique

It is clear that the elongation is affected by the deposition technique of SiO_2. At the highest applied fluence, ALD SiO_2 offers a higher elongation ratio than PECVD SiO_2. At lower fluences, the opposite happens. This could be at least partially explained by the fact that PECVD SiO_2 has a slightly higher density than the ALD SiO_2 and the presence of grains in PECVD SiO_2. When an irradiated material is denser, bigger energy loss occurs, resulting in greater deposited energy in the material and consequently greater elongation. Apart from the difference in the overall density between the two types of SiO_2, the dark halos surrounding the nanoparticles can be interpreted as regions with a higher density. Since these regions are much more distinct in PECVD SiO_2 than in ALD SiO_2, we assume that this layer has such a density, which enables the nanoparticle to elongate more in PECVD SiO_2. As a result, the underdensification happens faster in PECVD SiO_2 than in ALD SiO_2 until the fluence of 5×10^{13}. However, the elongation of nanoparticles embedded in PECVD SiO_2 saturates faster: for

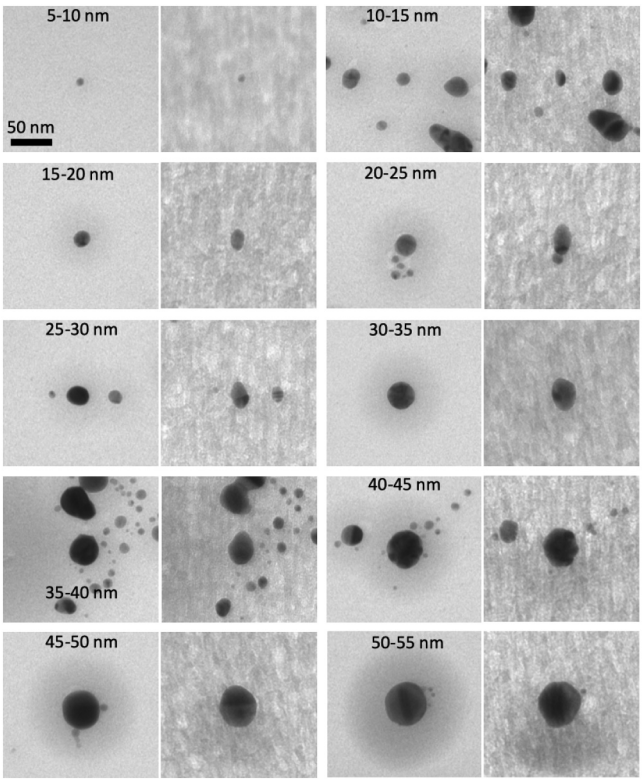

FIG. 16. TEM images of nanoparticles sandwiched between two 50 nm ALD SiO_2 layers (as-deposited). The samples were irradiated with ^{127}I at a fluence of 5×10^{13} ions/cm^2 before (left) and after (right) the irradiation.

5×10^{14} ions/cm^2 fluence, there is only a small increase in the elongation ratio compared to 5×10^{13} ions/cm^2 fluence. On the other hand, for ALD, the elongation ratio is significantly higher at 5×10^{14} ions/cm^2 fluence compared to 10^{14} ions/cm^2 fluence and to a PECVD sample at 5×10^{14} ions/cm^2 fluence. These findings imply that in the range between 5×10^{13} and 5×10^{14} ions/cm^2, the underdensification happens faster within the ALD type. The dark halos surrounding the nanoparticles in a PECVD type in combination with the grains appearing in this make the nanoparticles elongate less in PECVD type than in ALD, and the underdensification happens slower at the higher fluences.

C. Effect of annealing

Finally, regarding the effect of the annealing prior to irradiation, there is no significant difference in the elongation ratio at lower fluences. The biggest difference is observed at the highest applied fluence where the as-deposited sample seems not to withstand irradiation as almost all the windows were broken after the irradiation. The reason could be that annealing makes the material sustain more easily the plastic deformation during the irradiation and not break. The annealing step makes the SiO_2 coated TEM grids more durable.

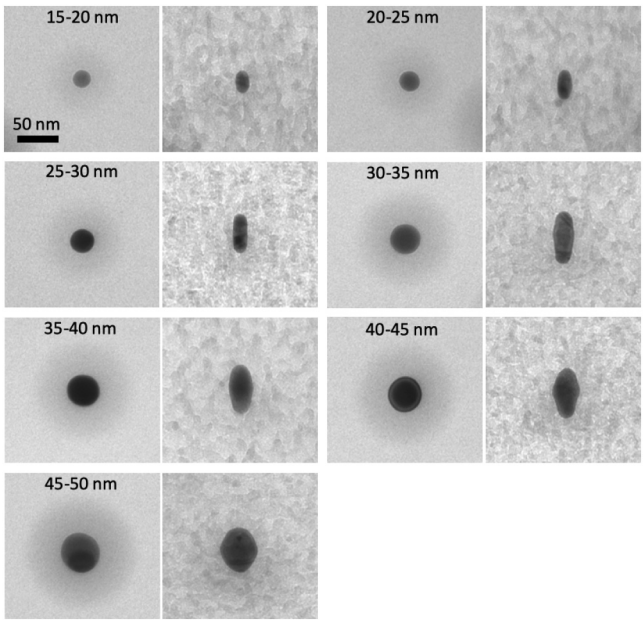

FIG. 17. TEM images of nanoparticles sandwiched between two 50 nm ALD SiO_2 layers (as-deposited). The samples were irradiated with ^{127}I at 10^{14} ions/cm^2 before (left) and after (right) the irradiation.

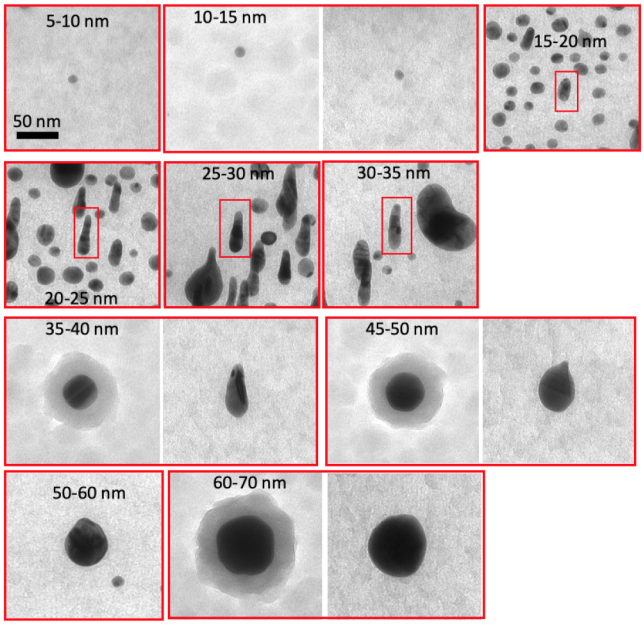

FIG. 18. TEM images of nanoparticles sandwiched between two 50 nm PECVD SiO_2 layers (annealed after the deposition). The samples were irradiated with ^{127}I at a fluence of 5×10^{14} ions/cm^2 before and after the irradiation. The red outline includes either a pair of nanoparticles before (left) and after (right) the irradiation or only nanoparticles after the irradiation.

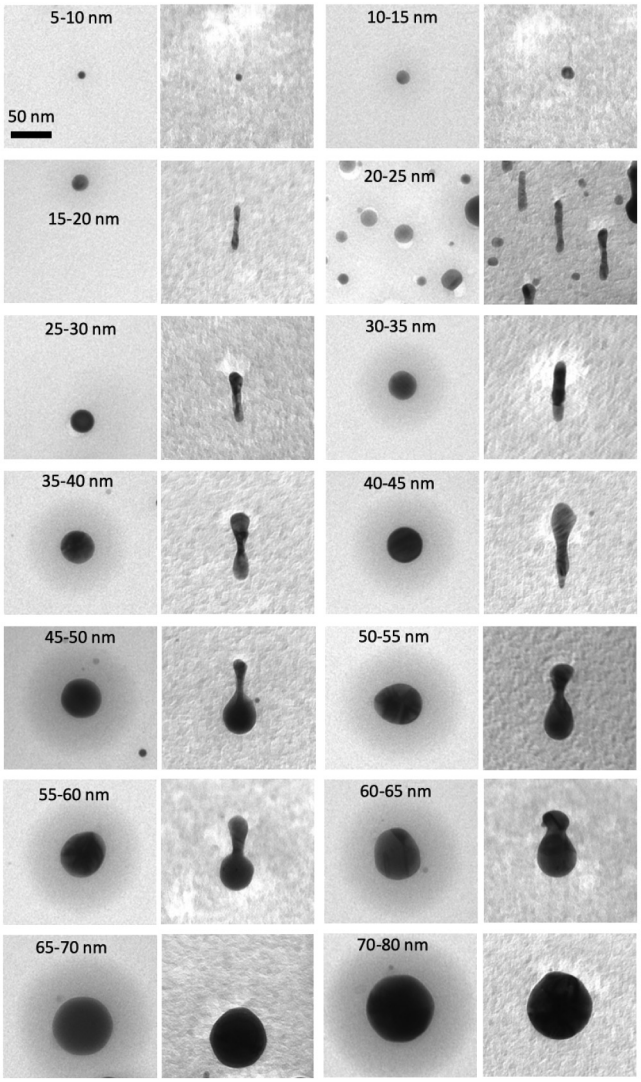

FIG. 19. TEM images of nanoparticles sandwiched between two 50 nm ALD SiO_2 layers (annealed after the deposition). The samples were irradiated with ^{127}I at a fluence of 5×10^{14} ions/cm^2 before (left) and after (right) the irradiation.

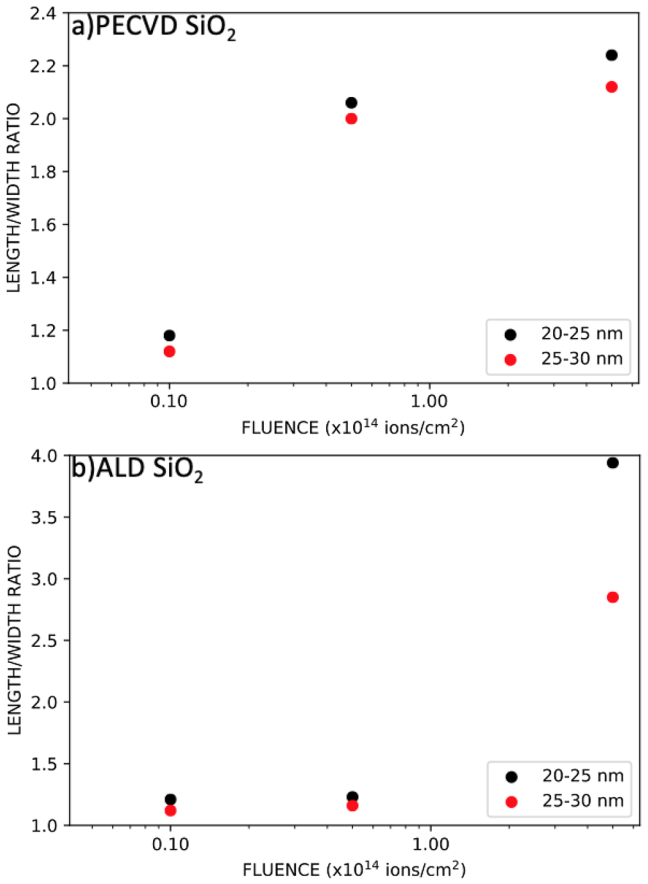

FIG. 20. Evolution of the elongation ratio with increasing fluence for two different nanoparticle sizes in (a) PECVD SiO_2 and (b) ALD SiO_2.

V. CONCLUSIONS

In this work, we investigated in detail the elongation of spherical gold nanoparticles of various diameters by imaging the same nanoparticles before and after the SHI irradiation. The deposition of SiO_2 by two techniques (ALD and PECVD) in combination with post-deposition annealing showed that the impact of the irradiation on nanoparticles depends on the deposition process of the samples, the quality of the SiO_2, and the size of the nanoparticles. Furthermore, the use of 20 nm Si_3N_4 TEM windows as a substrate makes it easier to study in detail the irradiation effect on nanostructures. Nanostructures of various sizes and shapes can be fabricated and imaged within the same sample in different phases of the processing, and their evolution can be followed.

ACKNOWLEDGMENTS

We gratefully acknowledge the Academy of Finland NANOIS project (Project No. 309730) for financial support. In addition, we especially thank Dr. Manu Lahtinen (Department of Chemistry, University of Jyväskylä) for his assistance in XRR measurements.

AUTHOR DECLARATIONS

Conflict of Interest

The authors have no conflicts to disclose.

Author Contributions

Spyridon Korkos: Conceptualization (lead); Investigation (lead); Methodology (lead); Software (lead); Validation (lead); Visualization (lead); Writing – original draft (lead).

Kenichiro Mizohata: Investigation (supporting). **Sami Kinnunen:** Investigation (supporting). **Timo Sajavaara:** Writing – review and editing (supporting). **Kai Arstila:** Conceptualization (equal); Investigation (equal).

DATA AVAILABILITY

The data that support the findings of this study are available from the corresponding author upon reasonable request.

REFERENCES

[1]C. d'Orléans, J. Stoquert, C. Estournes, C. Cerruti, J. Grob, J. Guille, F. Haas, D. Muller, and M. Richard-Plouet, "Anisotropy of Co nanoparticles induced by swift heavy ions," Phys. Rev. B **67**, 220101 (2003).

[2]S. Roorda, T. van Dillen, A. Polman, C. Graf, A. van Blaaderen, and B. J. Kooi, "Aligned gold nanorods in silica made by ion irradiation of core–shell colloidal particles," Adv. Mater. **16**, 235–237 (2004).

[3]Y. Mishra, F. Singh, D. Avasthi, J. Pivin, D. Malinovska, and E. Pippel, "Synthesis of elongated Au nanoparticles in silica matrix by ion irradiation," Appl. Phys. Lett. **91**, 063103 (2007).

[4]R. Giulian, P. Kluth, L. Araujo, D. Sprouster, A. Byrne, D. Cookson, and M. C. Ridgway, "Shape transformation of Pt nanoparticles induced by swift heavy-ion irradiation," Phys. Rev. B **78**, 125413 (2008).

[5]K. Awazu, X. Wang, M. Fujimaki, J. Tominaga, H. Aiba, Y. Ohki, and T. Komatsubara, "Synthesis of elongated Au nanoparticles in silica matrix by ion irradiation," Phys. Rev. B **78**, 054102 (2008).

[6]E. Dawi, A. Vredenberg, G. Rizza, and M. Toulemonde, "Ion-induced elongation of gold nanoparticles in silica by irradiation with Ag and Cu swift heavy ions: Track radius and energy loss threshold," Nanotechnology **22**, 215607 (2011).

[7]G. Rizza, P. E. Coulon, V. Khomenkov, C. Dufour, I. Monnet, M. Toulemonde, S. Perruchas, T. Gacoin, D. Mailly, X. Lafosse, C. Ulysse, and E. A. Dawi, "Rational description of the ion-beam shaping mechanism," Phys. Rev. B **86**, 035450 (2012).

[8]H. Amekura, S. Mohapatra, U. Singh, S. Khan, P. Kulriya, N. Ishikawa, N. Okubo, and D. Avasthi, "Shape elongation of Zn nanoparticles in silica irradiated with swift heavy ions of different species and energies: Scaling law and some insights on the elongation mechanism," Nanotechnology **25**, 435301 (2014).

[9]P.-E. Coulon, J. Amici, M.-C. Clochard, V. Khomenkov, C. Dufour, I. Monnet, C. Grygiel, S. Perruchas, C. Ulysse, L. Largeau, and G. Rizza, "Ion-shaping of embedded gold hollow nanoshells into vertically aligned prolate morphologies," Sci. Rep. **6**, 1 (2016).

[10]R. Li, K. Narumi, A. Chiba, Y. Hirano, D. Tsuya, S. Yamamoto, Y. Saitoh, N. Okubo, N. Ishikawa, C. Pang, F. Chen, and H. Amekura, "Matrix-material dependence on the elongation of embedded gold nanoparticles induced by 4 MeV C60 and 200 MeV Xe ion irradiation," Nanotechnology **31**, 265606 (2020).

[11]A. A. Leino, O. Pakarinen, F. Djurabekova, K. Nordlund, P. Kluth, and M. C. Ridgway, "Swift heavy ion shape transformation of Au nanocrystals mediated by molten material flow and recrystallization," Mater. Res. Lett. **2**, 37–42 (2014).

[12]T. Vu, C. Dufour, V. Khomenkov, A. Leino, F. Djurabekova, K. Nordlund, P.-E. Coulon, G. Rizza, and M. Hayoun, "Elongation mechanism of the ion shaping of embedded gold nanoparticles under swift heavy ion irradiation," Nucl. Instrum. Methods Phys. Res., Sect. B **451**, 42–48 (2019).

[13]H. Amekura, P. Kluth, P. Mota-Santiago, I. Sahlberg, V. Jantunen, A. Leino, H. Vazquez, K. Nordlund, and F. Djurabekova, "On the mechanism of the shape elongation of embedded nanoparticles," Nucl. Instrum. Methods Phys. Res., Sect. B **475**, 44–48 (2020).

[14]H. Amekura, N. Ishikawa, N. Okubo, M. C. Ridgway, R. Giulian, K. Mitsuishi, Y. Nakayama, C. Buchal, S. Mantl, and N. Kishimoto, "Zn nanoparticles irradiated with swift heavy ions at low fluences: Optically-detected shape elongation induced by nonoverlapping ion tracks," Phys. Rev. B **83**, 205401 (2011).

[15]O. Sánchez-Dena, P. Mota-Santiago, L. Tamayo-Rivera, E. García-Ramírez, A. Crespo-Sosa, A. Oliver, and J.-A. Reyes-Esqueda, "Size-and shape-dependent nonlinear optical response of Au nanoparticles embedded in sapphire," Opt. Mater. Express **4**, 92–100 (2014).

[16]A. Slablab, T. J. Isotalo, J. Mäkitalo, L. Turquet, P.-E. Coulon, T. Niemi, C. Ulysse, M. Kociak, D. Mailly, G. Rizza, and M. Kauranen, "Fabrication of ion-shaped anisotropic nanoparticles and their orientational imaging by second-harmonic generation microscopy," Sci. Rep. **6**, 37469 (2016).

[17]H. Amekura, K. Narumi, A. Chiba, Y. Hirano, K. Yamada, D. Tsuya, S. Yamamoto, N. Okubo, N. Ishikawa, and Y. Saitoh, "C_{60} ions of 1 MeV are slow but elongate nanoparticles like swift heavy ions of hundreds MeV," Sci. Rep. **9**, 14980 (2019).

[18]S. Schlücker, "Surface-enhanced Raman spectroscopy: Concepts and chemical applications," Angew. Chem. Int. Ed. **53**, 4756–4795 (2014).

[19]F. Tam, G. P. Goodrich, B. R. Johnson, and N. J. Halas, "Plasmonic enhancement of molecular fluorescence," Nano Lett. **7**, 496–501 (2007).

[20]P. Bharadwaj, B. Deutsch, and L. Novotny, "Optical antennas," Adv. Opt. Photonics **1**, 438–483 (2009).

[21]C. Clavero, "Plasmon-induced hot-electron generation at nanoparticle/metal-oxide interfaces for photovoltaic and photocatalytic devices," Nat. Photonics **8**, 95 (2014).

[22]R. Li, C. Pang, Z. Li, and F. Chen, "Plasmonic nanoparticles in dielectrics synthesized by ion beams: Optical properties and photonic applications," Adv. Opt. Mater. **8**, 1902087 (2020).

[23]P. Mota-Santiago, F. Kremer, A. Nadzri, M. C. Ridgway, and P. Kluth, "Elongation of metallic nanoparticles at the interface of silicon dioxide and silicon nitride," Nucl. Instrum. Methods Phys. Res., Sect. B **409**, 328–332 (2017).

[24]E. Dawi, W. ArnoldBik, R. Ackermann, and F. Habraken, "Shaping of Au nanoparticles embedded in various layered structures by swift heavy ion beam irradiation," Nucl. Instrum. Methods Phys. Res., Sect. B **384**, 86–92 (2016).

[25]P. Mota-Santiago, F. Kremer, G. Rizza, C. Dufour, V. Khomenkov, C. Notthoff, A. Hadley, and P. Kluth, "Ion shaping of single-layer Au nanoparticles in amorphous silicon dioxide, in silicon nitride, and at their interface," Phys. Rev. Mater. **4**, 096002 (2020).

[26]P.-E. Mota-Santiago, A. Crespo-Sosa, J.-L. Jiménez-Hernández, H.-G. Silva-Pereyra, J.-A. Reyes-Esqueda, and A. Oliver, "Size characterisation of noble-metal nano-crystals formed in sapphire by ion irradiation and subsequent thermal annealing," Appl. Surf. Sci. **259**, 574–581 (2012).

[27]S. Korkos, V. Jantunen, K. Arstila, T. Sajavaara, A. Leino, K. Nordlund, and F. Djurabekova, "Nanorod orientation control by swift heavy ion irradiation," Appl. Phys. Lett. **120**, 171602 (2022).

[28]J. Bachmann, R. Zierold, Y. T. Chong, R. Hauert, C. Sturm, R. Schmidt-Grund, B. Rheinländer, M. Grundmann, U. Gösele, and K. Nielsch, "A practical, self-catalytic, atomic layer deposition of silicon dioxide," Angew. Chem. Int. Ed. **47**, 6177–6179 (2008).

[29]D. Hiller, R. Zierold, J. Bachmann, M. Alexe, Y. Yang, J. W. Gerlach, A. Stesmans, M. Jivanescu, U. Müller, J. Vogt, H. Hilmer, P. Löper, M. Künle, F. Munnik, K. Nielsch, and M. Zacharias, "Low temperature silicon dioxide by thermal atomic layer deposition: Investigation of material properties," J. Appl. Phys. **107**, 064314 (2010).

[30]M. Zarchi, S. Ahangarani, and M. Z. Sanjari, "Properties of silicon dioxide film deposited by PECVD at low temperature/pressure," Metall. Mater. Eng. **20**, 89–96 (2014).

[31]X. Chen, Y. Lu, L. Tang, Y. Wu, B. J. Cho, X. Xu, J. Dong, and W. Song, "Annealing and oxidation of silicon oxide films prepared by plasma-enhanced chemical vapor deposition," J. Appl. Phys. **97**, 014913 (2005).

[32]J. Fu, H. Shang, Z. Li, W. Wang, and D. Chen, "Thermal annealing effects on the stress stability in silicon dioxide films grown by plasma-enhanced chemical vapor deposition," Microsyst. Technol. **23**, 2753–2757 (2017).

[33]M. Laitinen, M. Rossi, J. Julin, and T. Sajavaara, "Time-of-flight–energy spectrometer for elemental depth profiling–Jyväskylä design," Nucl. Instrum. Methods Phys. Res., Sect. B **337**, 55–61 (2014).
[34]K. Arstila, J. Julin, M. I. Laitinen, J. Aalto, T. Konu, S. Kärkkäinen, S. Rahkonen, M. Raunio, J. Itkonen, J.-P. Santanen, T. Tuovinen, and T. Sajavaara, "Potku–new analysis software for heavy ion elastic recoil detection analysis," Nucl. Instrum. Methods Phys. Res., Sect. B **331**, 34–41 (2014).
[35]M. R. Amirzada, A. Tatzel, V. Viereck, and H. Hillmer, "Surface roughness analysis of SiO_2 for PECVD, PVD and IBD on different substrates," Appl. Nanosci. **6**, 215–222 (2016).
[36]M. Kobylko, P.-E. Coulon, A. Slablab, A. Fafin, J. Cardin, C. Dufour, A. Losquin, M. Kociak, I. Monnet, D. Mailly, X. Lafosse, C. Ulysse, E. Garcia-Caurel, and G. Rizza, "Localized plasmonic resonances of prolate nanoparticles in a symmetric environment: Experimental verification of the accuracy of numerical and analytical models," Phys. Rev. Appl. **9**, 064038 (2018).
[37]A. Krasheninnikov and K. Nordlund, "Ion and electron irradiation-induced effects in nanostructured materials," J. Appl. Phys. **107**, 3 (2010).
[38]K. Heinig, T. Müller, B. Schmidt, M. Strobel, and W. Möller, "Interfaces under ion irradiation: Growth and taming of nanostructures," Appl. Phys. A **77**, 17–25 (2003).
[39]P. Kluth, B. Johannessen, G. J. Foran, D. Cookson, S. Kluth, and M. C. Ridgway, "Disorder and cluster formation during ion irradiation of Au nanoparticles in SiO_2," Phys. Rev. B **74**, 014202 (2006).
[40]G. Rizza, H. Cheverry, T. Gacoin, A. Lamasson, and S. Henry, "Ion beam irradiation of embedded nanoparticles: Toward an *in situ* control of size and spatial distribution," J. Appl. Phys. **101**, 014321 (2007).
[41]O. Peña-Rodríguez, A. Prada, J. Olivares, A. Oliver, L. Rodríguez-Fernández, H. G. Silva-Pereyra, E. Bringa, J. M. Perlado, and A. Rivera, "Understanding the ion-induced elongation of silver nanoparticles embedded in silica," Sci. Rep. **7**, 1 (2017).
[42]P. Kluth, R. Giulian, D. Sprouster, C. Schnohr, A. Byrne, D. Cookson, and M. Ridgway, "Energy dependent saturation width of swift heavy ion shaped embedded Au nanoparticles," Appl. Phys. Lett. **94**, 113107 (2009).